Electronic Supplementary Information

One-dimensional Amorphous Cobalt (II) Metal-organic Framework Nanowire for Efficient Hydrogen Evolution Reaction

Jie Dong,[a] Cuncai Lv,[b] Mark G. Humphrey,[c] Chi Zhang,[a] Zhipeng Huang[a*]*

a. School of Chemical Science and Engineering, Tongji University, Shanghai, 200092, P.R. China.

b. Key Laboratory of High-precision Computation and Application of Quantum Field Theory of Hebei Province, Hebei Key Lab of Optic-electronic Information and Materials, The College of Physics Science and Technology, Hebei University, Baoding 071002, P.R. China

c. Research School of Chemistry, Australian National University, Canberra, ACT 2601, Australia

* Corresponding author: * Chi Zhang, email: chizhang@tongji.edu.cn; * Zhipeng Huang, email: zphuang@tongji.edu.cn

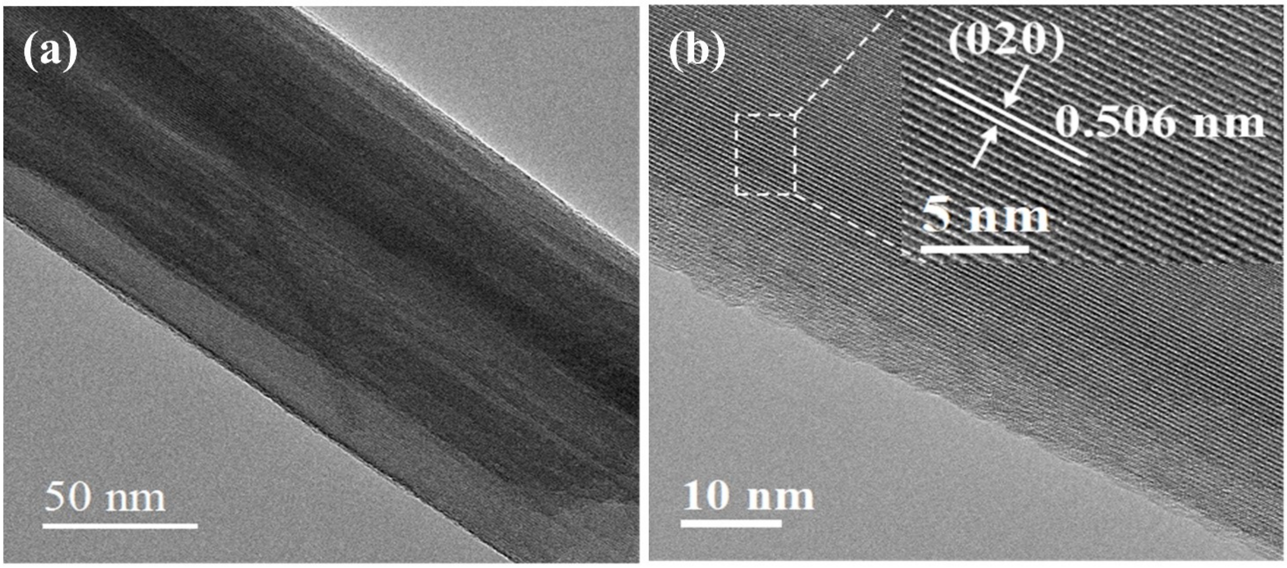

Fig. S1 TEM images of CoCH

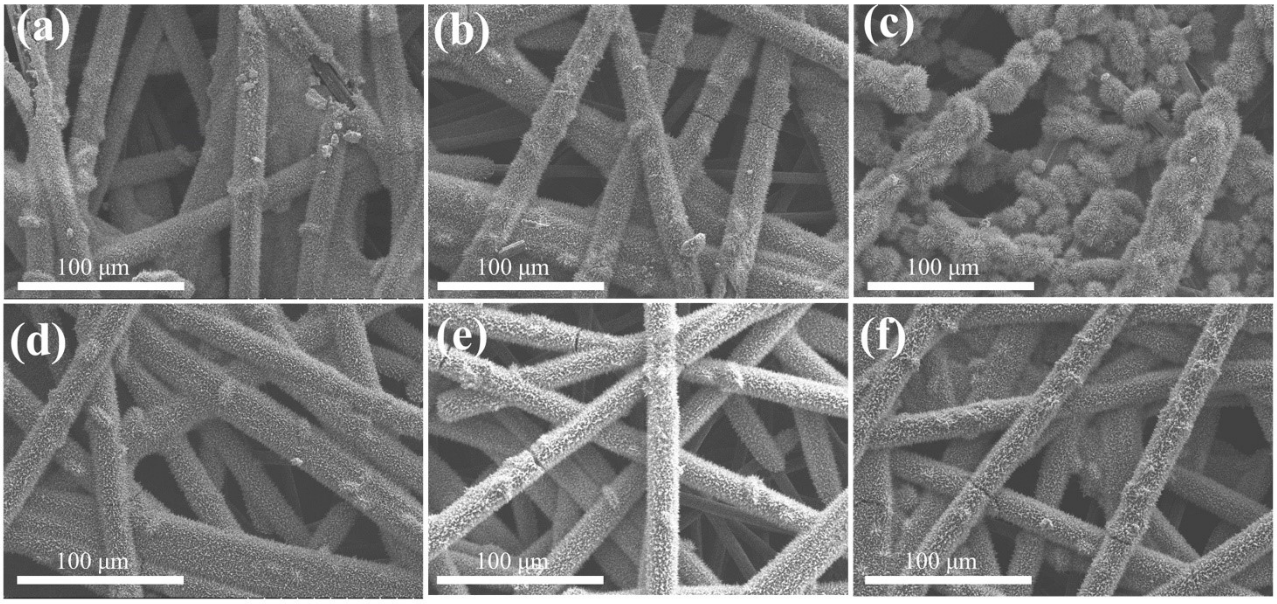

Fig. S2 SEM images of (a) CoCH@Co-MOF-10, (b) CoCH@Co-MOF-20, (c) CoCH@Co-MOF-30, (d) CoCH@Co-MOF-40, (e) CoCH@Co-MOF-50 and (f) CoCH@Co-MOF-60.

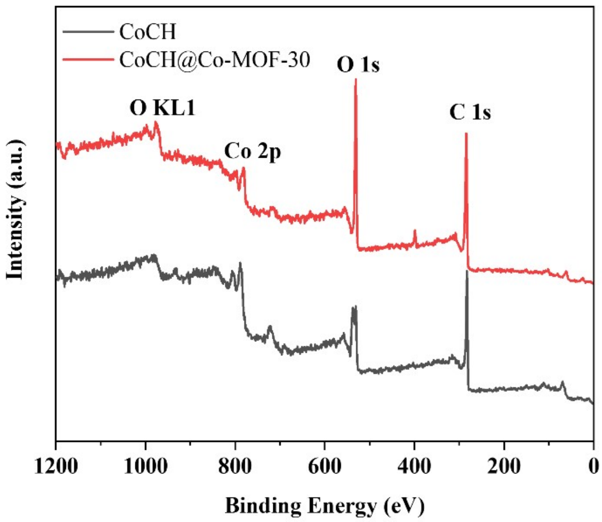

Fig. S3 XPS survey spectra of CoCH@Co-MOF-30 and CoCH.

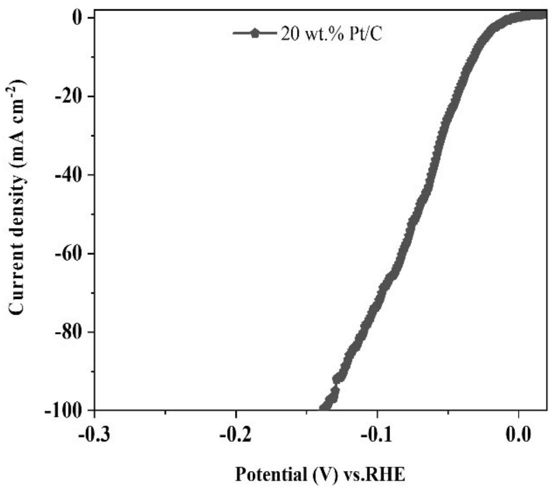

Fig. S4 LSV plots of commercial 20 wt.% Pt/C in 1.0 M KOH.

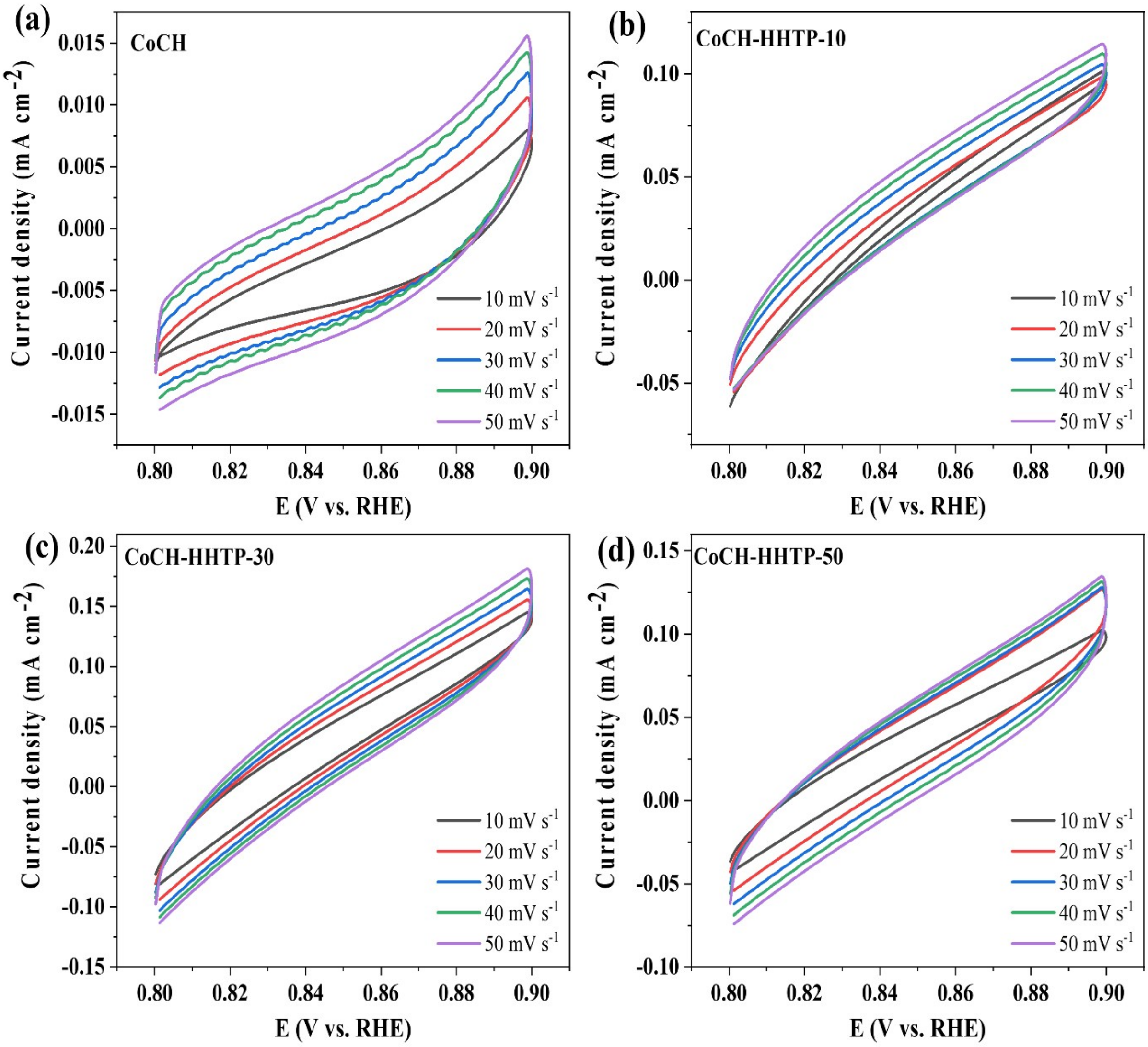

Fig. S5 CV curves at 0.8-0.9 V vs. RHE in 1.0 M KOH solution for (a) CoCH, (b) CoCH@Co-MOF-10, (c) CoCH@Co-MOF-30, and (d) CoCH@Co-MOF-50.

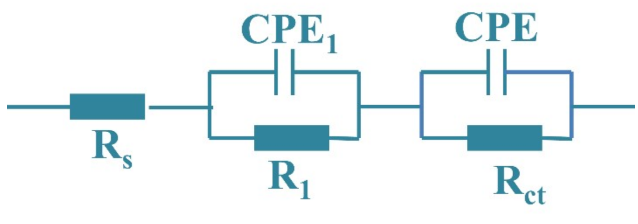

Fig. S6 The equivalent circuit model for electrochemical impedance tests. R_s, R_1, and R_{ct} represent the resistances of the electrolyte, electrode porosity, and charge transfer, respectively. The constant phase angle element (CPE) represents the double-layer capacitance of a solid electrode in a real-world situation.

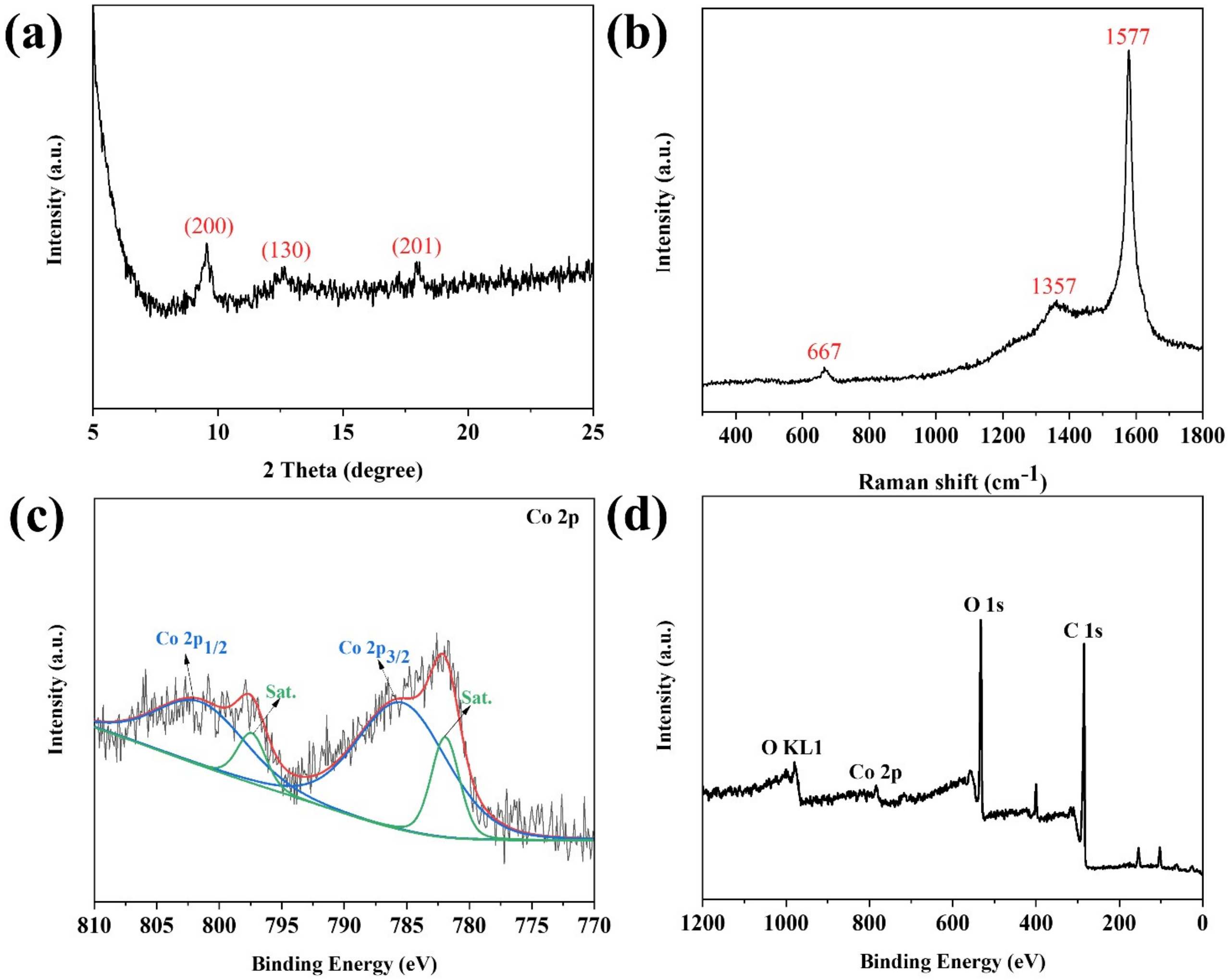

Fig. S7 (a) XRD pattern, (b) Raman spectrum, (c) High-resolution XPS spectra of Co 2p and (d) XPS survey spectrum of Co-MOF.

As shown in Fig. R1a, sharp peaks at 9.6°, 12.7°, and 18° refer to the crystalline facet of (200), (130), and (201)[1], respectively, indicating the good crystallinity of the Co-MOF. Raman spectra were recorded to further confirm the successful fabrication of as-prepared Co-MOF samples (Fig. R1b). The peaks detected at 667 cm^{-1} match well with Co-O coordination bonds in Co-MOF, while another broad peak around 1357 cm^{-1} is associated with ring stretching vibration of Co-MOF[2-3]. The peak at 1577 cm^{-1} can be assigned to H_2O. For the Co-MOF, the high-resolution XPS spectrum of Co 2p can be deconvoluted into four peaks shown in Fig. R1c, which are assigned to Co^{2+} (797.4 and 781.9 eV) and associated shakeup satellites (801.5 and 785.4 eV), respectively.[4]

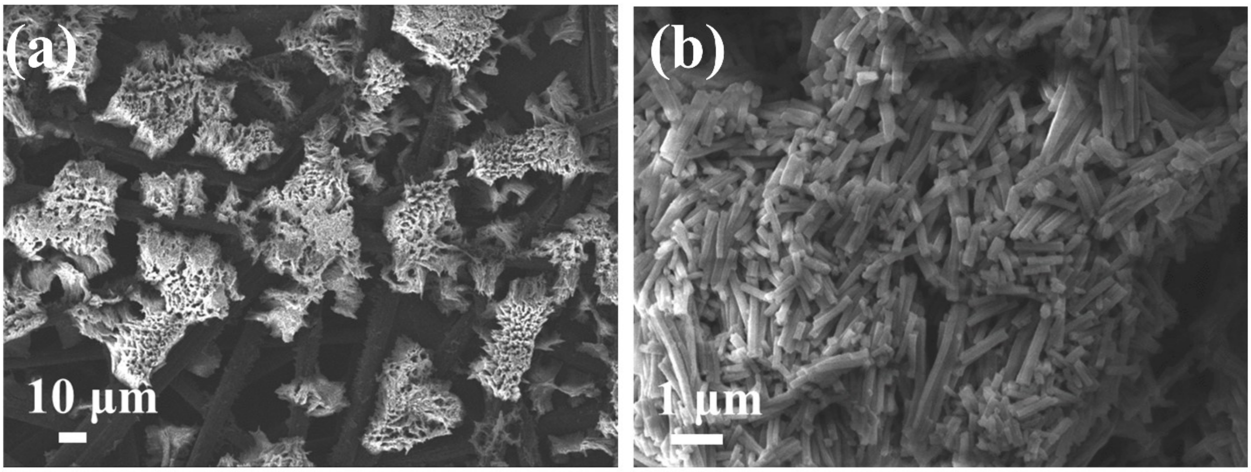

Fig. S8 (a-b) SEM images of Co-MOF.

The SEM image in Fig.R2 shows that numerous nanowires with high density homogeneously covering the carbon fiber papers. The TEM images are shown in Fig. R3. A lattice fringe pattern of a hexagonal crystal system is observed with a periodicity of ~1.82 nm, which corresponds to the (100) lattice planes of Co-MOF along the crystallographic c axis. The STEM elemental mapping of Co-MOF (Fig. R3c) shows the uniform spatial distribution of elemental C, O, and Co. Fig. R4 depicts the *iR*-corrected LSV plots of Co-MOF. The Co-MOF displays the electrocatalytic behavior with an overpotential of 358 mV *vs.* RHE for a cathodic current density of 10 mA cm^{-2}. It is obviously larger than that of CoCH@Co-MOF-30 (238 mV).

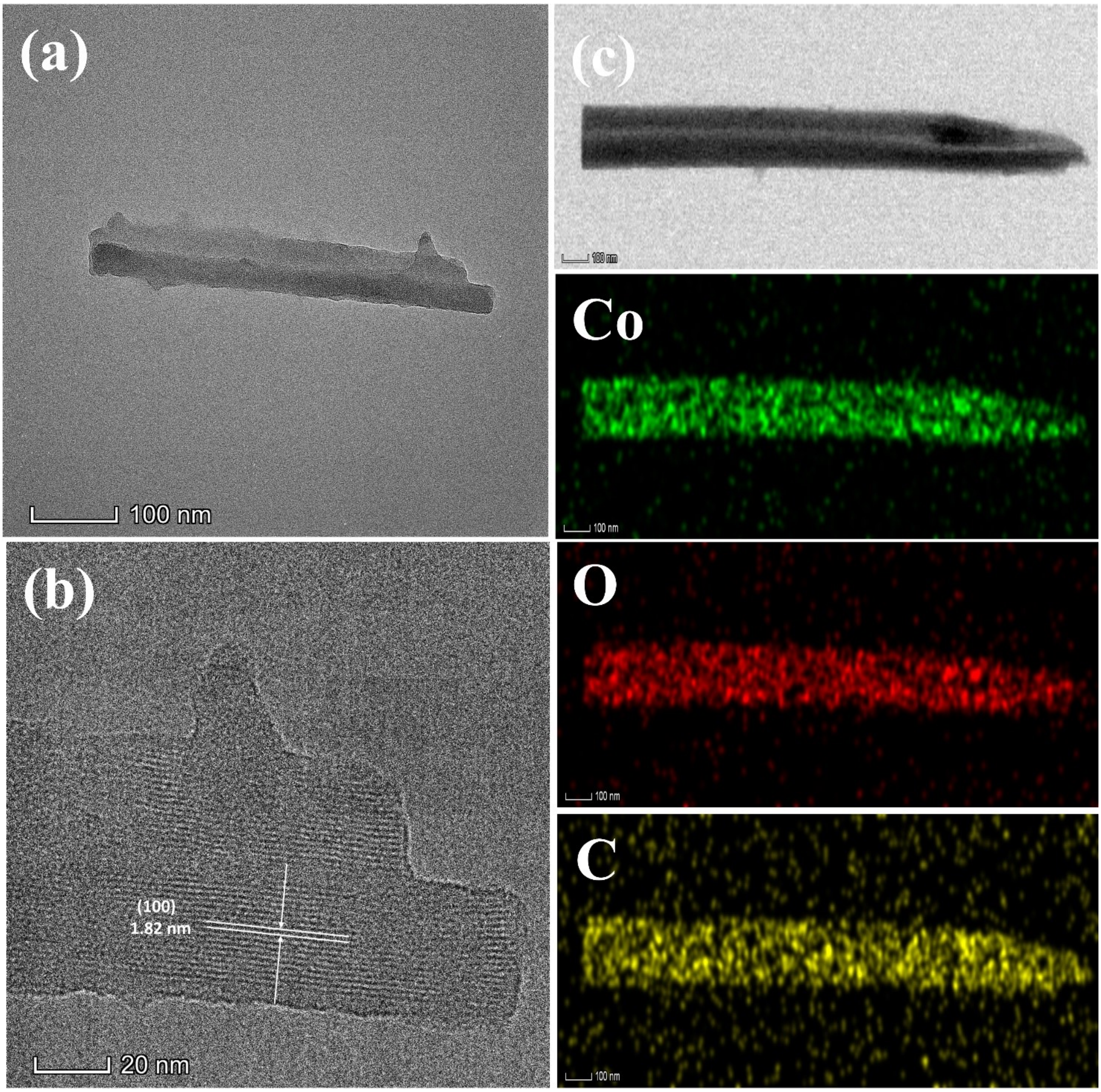

Fig. S9 (a - b) TEM images, (c) HADDF-STEM images and element mapping images of Co-MOF.

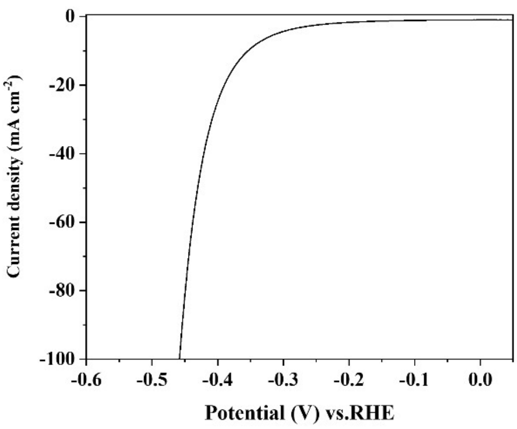

Fig. S10 LSV plots of Co-MOF in 1.0 M KOH.

Turnover frequency (TOF) calculation

The TOF values are calculated via the following equation[5]:

$$TOF = \frac{|j|A}{2nF}$$

Where $|j|$ is the current density at an overpotential of 300 mV during the LSV measurement in 1.0 M KOH solution. A stand for the area of the electrode (0.4 cm^2) and *F* is the Faradaic constant (96485 C mol^{-1}). 2 accounts for the electrons consumed to form H_2 molecule from water (2 electrons for hydrogen evolution reaction). *n* represents the quantity of active sites, and n can be calculated in as follows.

$$n = \frac{m_{cat} \times C_{wt\% - Co}}{M_{Co}}$$

If assuming all the Co ions take part in the electrocatalytic reaction, the value of *n* can be calculated based on the XPS results:

where m_{cat} is the catalyst loading on the carbon fiber cloth electrode (0.3 mg), $C_{wt\%}$ is the concentration of metal derived from XPS, the calculated n and *TOF* are as displayed in Table R1.

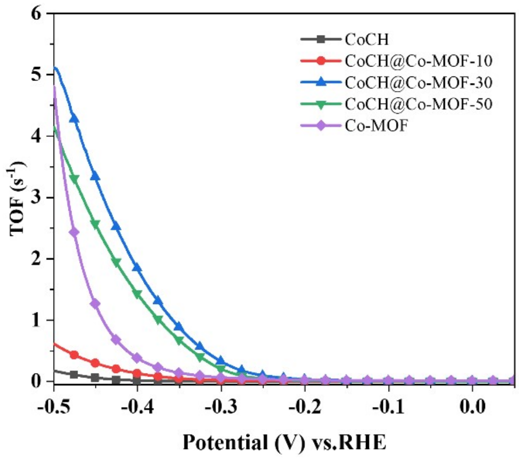

Fig.S11 Turnover frequency at 300 mV (vs. RHE) of different catalysts.

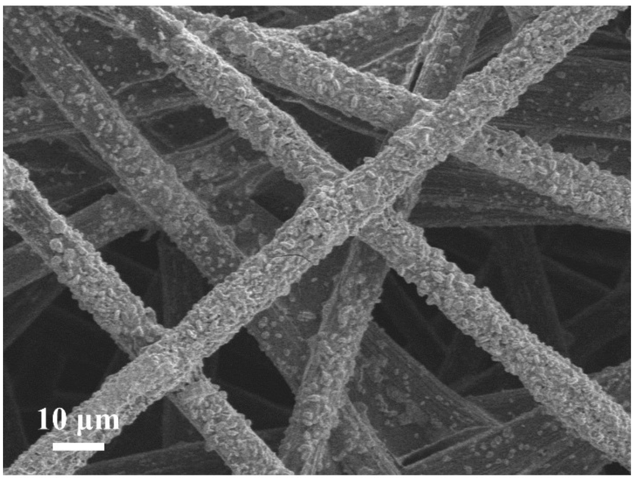

Fig. S12 SEM image of CoCH@Co-MOF-30 after HER durability test.

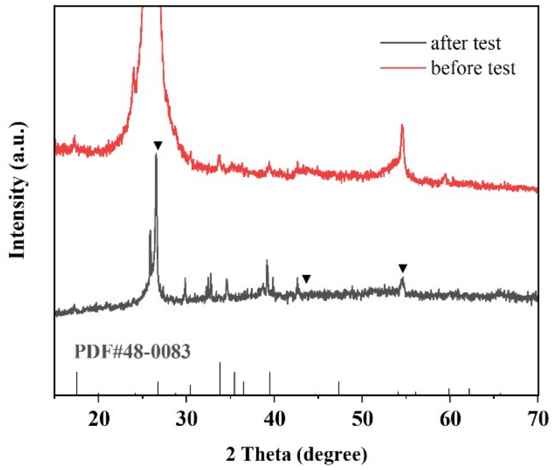

Fig. S13 XRD patterns of CoCH@Co-MOF-30 before and after HER durability test.

Table S1 Comparison of the TOF of different samples.

Sample	TOF (S^{-1})
CoCH	0.004
CoCH@Co-MOF-10	0.228
CoCH@Co-MOF-30	0.331
CoCH@Co-MOF-50	0.207
Co-MOF	0.067

Table S2 Summary of HER performance for some reported MOF-based electrocatalysts in alkaline solution.

Catalyst	Counter electrode	Scan rate (mv s^{-1})	η_{10}	Tafel slope (mV dec^{-1})	Ref.
$Fe(OH)_x$@Cu-MOF[a]	graphite rod	5	112	76	[6]
Ni-MOF/Ni_2P@EG[a]	graphite rod	5	132	59	[7]
Ni-MOF@Pt (20 wt % Pt) [a]	Pt mesh	5	102	88	[8]
NiFe-MS/MOF@NF[a]	graphite rod	2	156[c]	82	[9]
Pt/MOF-O[a]	carbon rod	5	66	24	[10]
Co_3S_4/EC-MOF[a]	carbon rod	1	84	82	[11]
Pt-NC/Ni-MOF[a]	graphite rod	-	25	42	[12]
Fe doped MOF CoV@CoO[a]	platinum wire	5	78	52	[13]
CuCo-CAT/CC[a]	graphite rod	5	52	52	[14]
$NiRu_{0.13}$-BDC[a]	carbon rod	2	34	32	[15]
$Ni_3(Ni_3{\cdot}HAHATN)_2$ MOF[b]	graphite	5	115	45	[16]
MFN-MOFs[a]	graphite plate	0.5	79	30	[17]
FePc@Ni-MOF[b]	graphite rod	10	334	72	[18]
NiRu-MOF/NF[a]	graphite rod	5	51	90	[19]
Fe_2Zn-MOF[b]	platinum wire	5	221	174	[20]
Co-BDC/MoS_2[a]	graphite rod	5	248	86	[21]
CoS_x/Co-MOF[a]	carbon rod	5	73	83	[22]
CoCH@Co-MOF-30[a]	graphite rod	5	238	95	the work

Note: η_{10}, overpotential (mV) at 10 mA cm^{-2}; the unit of Tafel slope is mV dec^{-1}. [a] The HER performance of catalysts is measured in 1.0 M KOH solution. [b] The HER performance of catalysts is measured in 0.1 M KOH solution. [c] The overpotential at 50 mA cm^{-2}.

Refereces

1. Y. Shi, M. R. Momeni, Y.-J. Chen, Z. Zhang and F. A. Shakib, Water-Induced Structural Transformations in Flexible Two-Dimensional Layered Conductive Metal–Organic Frameworks, *Chem. Mater.,* 2020, **32**, 9664-9674.
2. X. Liu, M. Zhuo, W. Zhang, M. Gao, X. H. Liu, B. Sun and J. Wu, One-step ultrasonic synthesis of Co/Ni-catecholates for improved performance in oxygen reduction reaction, Ultrason. *Sonochem.*, 2020, **67**, 105179.
3. L. Tang, J. Shi, X. Wang, S. Zhang, H. Wu, H. Sun and Z. Jiang, Coordination polymer nanocapsules prepared using metal-organic framework templates for pH-responsive drug delivery, *Nanotechnology*, 2017, **28**, 275601.
4. J. Sun, L. Guo, X. Sun, J. Zhang, Y. Liu, L. Hou and C. Yuan, Conductive Co-based metal–organic framework nanowires: a competitive high-rate anode towards advanced Li-ion capacitors, *J. Mater. Chem. A*, 2019, **7**, 24788-24791.
5. J. Zhou, Z. Han, X. Wang, H. Gai, Z. Chen, T. Guo, X. Hou, L. Xu, X. Hu, M. Huang, S. V. Levchenko and H. Jiang, Discovery of Quantitative Electronic Structure-OER Activity Relationship in Metal-Organic Framework Electrocatalysts Using an Integrated Theoretical-Experimental Approach, *Adv. Funct. Mater.*, 2021, **31**, 2102066.
6. W. Cheng, H. Zhang, D. Luan and X. W. D. Lou, Exposing unsaturated Cu_1-O_2 sites in nanoscale Cu-MOF for efficient electrocatalytic hydrogen evolution, *Sci. Adv.*, 2021, **7**, eabg2580.
7. F. Cheng, L. Wang, H. Wang, C. Lei, B. Yang, Z. Li, Q. Zhang, L. Lei, S. Wang and Y. Hou, Boosting alkaline hydrogen evolution and Zn–H_2O cell induced by interfacial electron transfer, *Nano Energy*, 2020, **71**, 104621.
8. K. Rui, G. Zhao, M. Lao, P. Cui, X. Zheng, X. Zheng, J. Zhu, W. Huang, S. X. Dou and W. Sun, Direct hybridization of noble metal nanostructures on 2D metal-organic framework nanosheets to catalyze hydrogen evolution, *Nano Lett.*, 2019, **19**, 8447-8453.
9. M. Zhao, W. Li, J. Li, W. Hu and C. M. Li, Strong electronic interaction enhanced electrocatalysis of metal sulfide clusters embedded metal-organic framework ultrathin nanosheets toward highly efficient overall water splitting, *Adv. Sci.*, 2020, **7**, 2001965.
10. M. Wang, Y. Xu, C. K. Peng, S. Y. Chen, Y. G. Lin, Z. Hu, L. Sun, S. Ding, C. W. Pao, Q. Shao and X. Huang, Site-specified two-dimensional heterojunction of Pt nanoparticles/metal-organic frameworks for enhanced hydrogen evolution, *J. Am. Chem. Soc.*, 2021, **143**, 16512-16518.
11. T. Liu, P. Li, N. Yao, T. Kong, G. Cheng, S. Chen and W. Luo, Self-sacrificial template-directed vapor-phase growth of MOF assemblies and surface vulcanization for efficient water splitting, *Adv. Mater.*, 2019, **31**, 1806672.
12. C. Guo, Y. Jiao, Y. Zheng, J. Luo, K. Davey and S.-Z. Qiao, Intermediate modulation on noble metal hybridized to 2D metal-organic framework for accelerated water electrocatalysis, *Chem*, 2019, **5**, 2429-2441.
13. Muthurasu, A. P. Tiwari, K. Chhetri, B. Dahal and H. Y. Kim, Construction of iron doped cobalt- vanadate- cobalt oxide with metal-organic framework oriented nanoflakes for portable rechargeable zinc-air batteries powered total water splitting, *Nano Energy*, 2021, **88**, 106238.
14. Geng, F. Yan, X. Zhang, Y. He, C. Zhu, S. L. Chou, X. Zhang and Y. Chen, Conductive CuCo-based bimetal organic framework for efficient hydrogen evolution, *Adv. Mater.*, 2021, **33**, 2106781.
15. Y. Sun, Z. Xue, Q. Liu, Y. Jia, Y. Li, K. Liu, Y. Lin, M. Liu, G. Li and C. Y. Su, Modulating electronic structure of metal-organic frameworks by introducing atomically dispersed Ru for efficient hydrogen evolution, *Nat. Commun*., 2021, **12**, 1369.
16. H. Huang, Y. Zhao, Y. Bai, F. Li, Y. Zhang and Y. Chen, Conductive metal-organic frameworks with extra metallic sites as an efficient electrocatalyst for the hydrogen evolution reaction, *Adv. Sci.*, 2020, **7**, 2000012.
17. D. Senthil Raja, H.-W. Lin and S.-Y. Lu, Synergistically well-mixed MOFs grown on nickel foam as highly efficient durable bifunctional electrocatalysts for overall water splitting at high current densities, *Nano Energy*, 2019, **57**, 1-13.
18. Y. Xu, S. Yu, T. Ren, S. Liu, Z. Wang, X. Li, L. Wang and H. Wang, Hydrophilic/aerophobic hydrogen-evolving electrode:

NiRu-based metal-organic framework nanosheets in situ grown on conductive substrates, *ACS Appl. Mater. Interfaces*, 2020, **12**, 34728-34735.

19. X. Zhang, R. Lin, X. Meng, W. Li, F. Chen and J. Hou, Iron phthalocyanine/two-dimensional metal-organic framework composite nanosheets for enhanced alkaline hydrogen evolution, *Inorg. Chem.*, 2021, **60**, 9987-9995.
20. M. Gu, S. C. Wang, C. Chen, D. Xiong and F. Y. Yi, Iron-based metal-organic framework system as an efficient bifunctional electrocatalyst for oxygen evolution and hydrogen evolution reactions, *Inorg. Chem.*, 2020, **59**, 6078-6086.
21. D. Zhu, J. Liu, Y. Zhao, Y. Zheng and S. Z. Qiao, Engineering 2D metal-organic framework/MoS_2 interface for enhanced alkaline hydrogen evolution, *Small*, 2019, **15**, 1805511.
22. W. Zhou, Z. Xue, Q. Liu, Y. Li, J. Hu and G. Li, Trimetallic MOF-74 films grown on Ni foam as bifunctional electrocatalysts for overall water splitting, *ChemSusChem*, 2020, **13**, 5647-5653.